Atomic structure of hardening precipitates in an Al–Mg–Zn–Cu alloy determined by HAADF-STEM and first-principles calculations: relation to η-MgZn$_2$

**Calin D. Marioara · Williams Lefebvre ·
Sigmund J. Andersen · Jesper Friis**

Abstract The structures of two nanoscale plate precipitates prevalent at maximum strength and over-aged conditions in a 7449 Al–Mg–Zn–Cu alloy were investigated. Models derived from images of high angle annular dark field scanning transmission electron microscopy were supported by first-principles calculations. Both structures are closely linked to the η-MgZn$_2$ Laves phase through similar layers of a rhombohedral atomic subunit. The finest plate contains one such layer together with a layer of an orthorhombic unit. The second plate contains rhombohedral layers only, normally four, but rotated relatively to form different stacking variants, one of which may be likened to η. For both structures, the same atomic planes describe the main interface with Al. Both plates could be described in space group P3. The unit cells comprise interface and arbitrary numbers of {111}Al (habit) planes. Eight Al-planes were included in the first-principles calculations. The enthalpy indicates high layer/unit stability. The plate thickness can be understood by a simple mismatch formulation.

Introduction

The age-hardenable Al–Mg–Zn–(Cu) alloys are highly important for automotive and aerospace structural purposes, in particular because of their high strength/weight ratio. The hardening takes place during a final ageing step, after a quench from high temperature has brought the solute into supersaturated solid solution. The solute forms clusters, of which a fraction turns into fully coherent Guinier–Preston (GP) zones upon ageing, with atoms still restricted to the Al lattice. With continued ageing semi-coherent precipitates appear, called η'. Both phases are nanoscale plates forming on {111}Al planes. Maximum strength coincides with a combined high number density of GP-zones and η', reached after a few hours of ageing. Longer times lead to coarsening, characterized by reduced precipitate numbers of the plate-like equilibrium phase η-MgZn$_2$, accompanied by coherency and strength losses. The precipitation sequence is given as [1–3]

$$SSSS \ \rightarrow \ GP - zones \ \rightarrow \ \eta' \rightarrow \ \eta. \tag{1}$$
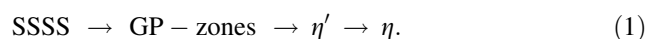
The sizes of the smallest precipitates and their inseparability from the aluminium have prevented accurate experimental determination of atomic structure and composition. Based on transmission electron microscopy (TEM) techniques, several atomic models have been proposed for the η'-phase [4–8]. Unfortunately, first-principles calculations have indicated high formation enthalpies, casting some doubt on their correctness [9]. This reflects the problems associated with TEM techniques, such as insufficient spatial and elemental resolution, and are caused by dynamic scattering, small precipitate size and to overlap with the Al matrix [6–8]. Even precise estimates of plate thickness can be difficult because images are strongly influenced by strain, and since the traditional imaging methods such as bright field or high resolution TEM (HRTEM) generally lack atom specific contrast. For example, thickness can be underestimated by non-detectable solute atoms ordering on 'the Al planes outside the precipitate', or the surrounding local strain field modifies

C. D. Marioara · S. J. Andersen (✉) · J. Friis
SINTEF Materials and Chemistry, Høgskoleringen 5,
7465 Trondheim, Norway
e-mail: sigmund.j.andersen@sintef.no

W. Lefebvre
Groupe de Physique des Matériaux, UMR CNRS 6634, Institut des Matériaux de Rouen, Site Universitaire du Madrillet, Université de Rouen, 76801 Saint Etienne du Rouvray CEDEX, France

scattering which can lead to overestimation. Selected area diffraction is also strongly effected by interface structure and strain in such small precipitates. If several types and variants exist, as is one conclusion in this study, interpreting structure by statistical diffraction methods [7] can be quite challenging. Thus, only the structure of η-MgZn$_2$, as solved by standard X-ray [10] diffraction techniques, is known within certainty. A recent reinvestigation [11] of η confirms its unit cell to contain four units of MgZn$_2$, to have parameters $a = b = 0.522$ nm, $c = 0.857$ nm and space group P6$_3$/mmc (194). It is known as a polytype (C14) of the Laves phases, and is a most common intermetallic structure type. A main characteristic of a Laves phase is its layered nature, where layers are built by a few atomic planes [12]. A number of polytypes can be explained from different stackings of these layers; a combination of identical layers may stack on top of each other, or being mixed with 180° rotated layers about the (hexagonal) layer normal. Although it will become clear that some or all the precipitates described here may qualify as Laves phases, we shall not pursue this further. The reason is that the precipitates are here integrated in the Al matrix, suggesting the interface should be considered together with the bulk structure. Recent atom probe tomography (APT) studies have indicated that the composition of the metastable precipitates in the Al–Mg–Zn(–Cu) system vary with alloy composition and heat treatment [3, 13–18]. Zn/Mg ratios between 0.9 and 1.4 have been found, well below the pre-assumed equilibrium MgZn$_2$ concentration. The elements Cu and Al have been shown to enter into the precipitates [3, 13, 15, 16]. Future studies, which should better account for evaporation artefacts [19] will most likely improve the accuracy.

The contrast in images of the spherical aberration (Cs) probe corrected HAADF-STEM instruments is generally unaffected by small changes in the objective lens defocus and specimen thickness [20–22]. With the Z-contrast and a spatial resolution towards 0.1 nm, the method therefore has the advantage of providing more directly interpretable images as compared to HRTEM. The high spatial resolution and superior signal-to-noise ratio can enable discrimination even between neighbour elements, such as Al and Mg, which is of high value for the present work. In a recent HAADF-STEM investigation [23], the precipitates in an Al–Mg–Zn alloy were imaged with the Al matrix oriented along $\langle 110 \rangle$ Al. However, no particular η' phase could be identified. Instead, the authors found the HAADF-STEM simulations matched the equilibrium η-phase the best.

In this work, we focus on the atomic structures of two coherent nanoscale plate precipitates phases existing in high numbers at peak- and over-aged conditions in a commercial Al–Mg–Zn–Cu alloy. Aberration-corrected HAADF-STEM was used to establish models which were subsequently evaluated by first-principles calculations. As

the plates reside on {111}Al planes, they need to be viewed normal to the $\langle 111 \rangle$ Al plate normal, to have sufficient number of atoms in the analysed precipitate columns, and to limit the overlap with the aluminium. Li et al. [23] imaged the precipitates along an $\langle 110 \rangle$ Al direction. Here, it was decided to use $\langle 112 \rangle$ Al instead due to the larger inter-columnar separation in this projection.

Experimental procedure

The investigated alloy with designation AA7449 had nominal composition 8.5 % Zn, 2.2 % Mg, 1.9 % Cu, 0.08 % Fe, 0.06 % Si and 0.13 % (Zr + Ti), all in wt%. The as-received material, in the form of rolled plates 25-mm thick, had a fibrous grain structure. A T6 condition (temper) was produced as follows; 6 h solution heat treatment at 470 °C, quenching by water spray, 2 % stretching, 4 days storage at Room Temperature (RT), and ageing for 22 h at 120 °C. The heating rate from RT to 120 °C was 30 °C/h. The T7 condition was achieved by a 6 h solution heat treatment at 473 °C, water spray quenching, 2 % stretching, 5 days storage at RT, ageing 6 h at 120 °C and ageing for 25 h at 150 °C. The heating rate from RT to 120 °C was 30 °C/h and the heating rate from 120 °C to 150 °C was 15 °C/h.

TEM specimens were prepared by electropolishing using a Tenupol 3 machine. The electrolyte consisted of 1/3 HNO$_3$ + 2/3 methanol and the solution was kept at a temperature between −20 and −35 °C.

A spherical aberration (Cs) probe corrected JEOL ARM200F scanning transmission electron microscope, operating at 200 kV was used to obtain the HAADF-STEM images. The probe size was set to 0.1 nm with a convergence semi-angle of 22.5 mrad. The collection angle of the HAADF detector was in the range of 45–150 mrad.

For the higher magnification HAADF-STEM images in Figs. 2 and 5 (based on the raw images in Fig. 1), to remove noise all features smaller than 0.13 nm were suppressed using fast fourier transform filtering.

HAADF-STEM image formation is the result of an incoherent process that may be described as a convolution of an object function and the electron probe intensity [24], where the object function represents the projected structure (position and nature of atomic columns). A de-convolution, following normal procedure [24] was performed on Fig. 1d, which allowed for more detailed quantification of the columns (presented in Fig. 3).

The first-principles calculations were performed at zero Kelvin with the Vienna ab initio simulation package (VASP) [25] using orthogonal super-cells that included 8 outer pure matrix (111)Al planes, corresponding to 1.887 nm separations between the periodic image of the
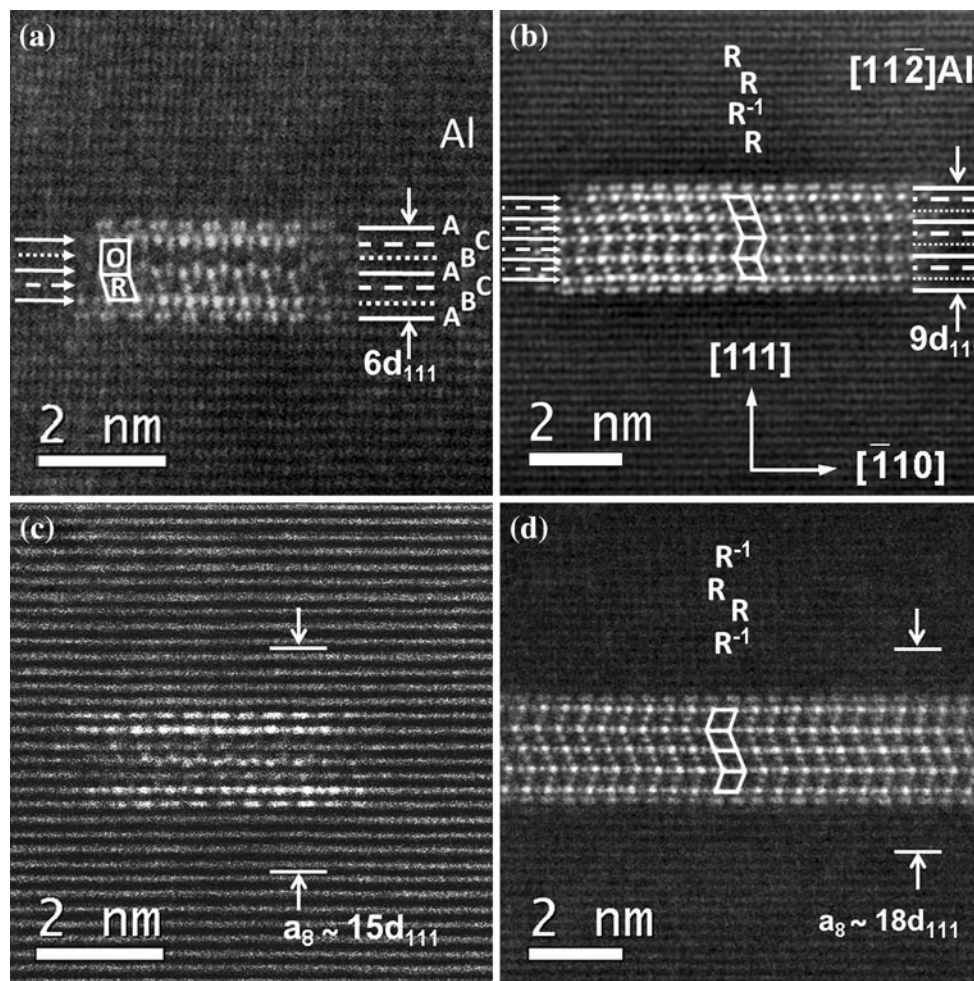
Fig. 1 $\langle 112 \rangle$ Al zone HAADF-STEM images of the two most abundant, coherent precipitates in conditions T6 (**a**, **b**) and T7 (**c**, **d**). Coordination system choice (**b**) applies to all images. *Arrows* (*left*): three (**a**) and two (**b**) different planes define *inner* parts. *Lines* (*right*) indicate Al (ABC) stacking. Type 1 (a, c) and Type 2 (b, d) contain layers of units with rhombic (R) projections (a-b, d). Type 1 has one layer of orthorhombic units (O) and one R-layer (**a**). Layers connect to Al through identical solute-enriched (111)Al *interface* planes (*outer solid* 'A' *lines*) (**a**, **b**). Type 2 stacking variants (b, d) are overlaid with rhombs 'R' and 'R^{-1}' (R^{-1} rotated 180° about [111]Al). Unit cell parameters a_l with $l = 8$ integrated Al-planes used for first-principles refinements are indicated for both precipitates in (**c**, **d**)

precipitates along [111]Al. No magnetic calculations were included. The initial atomic models for the precipitates were extracted in space group P1 using the information (atom types, inter-atomic distances and cell parameters) provided by the HAADF-STEM images, and the observed similarities with the equilibrium η-MgZn$_2$ phase. Atomic coordinates and unit cell parameters were refined. In all cases, Perdew–Burke–Ernzerhof functionals [26] were employed with plane wave cutoff of 277 eV, a Γ-centred Monkhorst–Pack k-point grid of $1 \times 3 \times 6$ and projected augmented-wave pseudo-potentials, relaxing the forces on all atoms to less than 0.05 eV/Å. In the refinements, both cell parameters and atom positions were relaxed by means of the quasi-Newton RMM-DIIS algorithm [27]. A convergence test using higher cutoff energies were checked (up to 500 eV), but higher cutoff was found to not change

energies appreciably and had no influence on the ranking of the structures as listed in Table 1.

Results

Two different plate-shaped precipitates, coherent with the aluminium matrix, were identified in high numbers in both the T6 (peak aged) and the T7 (over-aged) tempers. A qualitative comparison of images of similar magnifications showed that a coarser microstructure exists in T7 with larger precipitates and a lower number density. Relative or absolute fractions have not been measured. However, a rough estimate (based on 38 imaged precipitates in T6 and only 12 precipitates in T7) sets the relative number of plates (Type 1/Type 2) in T6 to just below unity. This ratio

Table 1 Formation enthalpies and relaxed parameters for orthogonal cell models of Type 1 (1a_pq and 1b_pq), and two stacking variants of Type 2 (2, 2_η)

Refined model types nx_pq and bulk η	Formation enthalpy per atom (eV/atom)	Formation enthalpy/ volume (eV/nm^3)	Refined cell parameters [nm] except for η-phase, 8 Al (111) planes were added			Model composition for $a = a_0$ (without external Al planes)		
			$a = a_8$	b	c	Al	Mg	Zn
1a_AlAl	−0.1260	−7.8	3.4523	0.8763	0.4978	8	8	28
1a_AlMg	−0.1670	−10.3	3.4011	0.8838	0.5051	4	12	28
1a_MgAl	−0.1477	−9.0	3.4605	0.878	0.5017	4	12	28
1a_MgMg	−0.1867	−11.3	3.4443	0.8847	0.505	0	16	28
1a_ZnAl	−0.1416	−8.8	3.3791	0.8818	0.5032	4	8	32
1a_ZnMg	−0.1824	−11.3	3.4084	0.8844	0.5008	0	12	32
1b_AlAl	−0.0922	−5.5	3.4595	0.8706	0.4972	6	8	28
1b_AlMg	−0.1238	−7.3	3.4241	0.8757	0.5027	2	12	28
1b_MgAl	−0.1137	−6.8	3.3888	0.8815	0.5033	4	10	28
1b_MgMg	−0.1380	−8.1	3.423	0.8785	0.5041	0	14	28
1b_ZnAl	−0.0981	−5.9	3.3932	0.879	0.5004	4	8	30
1b_ZnMg	−0.1315	−7.8	3.4364	0.8753	0.500	0	12	30
Type 2	−0.2100	−13.1	4.1613	0.8854	0.5085	0	20	46
Type 2_η	−0.2108	−13.2	4.1705	0.8857	0.5069	0	20	46
η-MgZn$_2$ nominal	−0.2182	−12.9	0.522	0.522	0.857	0	4	8
η-MgZn$_2$ relaxed	−0.2190	−13.4	0.5172	0.5172	0.8492	0	4	8

All include eight (111)Al planes ($a = a_8$). Two last rows: Enthalpies of bulk η-MgZn$_2$ (hexagonal) with nominal and relaxed parameters. '1a' and '1b' refer to Type 1 models of Fig. 5a, b, respectively. 'p' and 'q' refer to two sites (occupied by Al, Mg or Zn) in the centre of the orthorhombic unit, as indicated in the same figures. Cell parameter $a = a_0$ approximates $7d_{111}^{Al} = 1.637$ nm and $10d_{111}^{Al} = 2.338$ nm, for Type 1 and Type 2, respectively (see Fig. 1a, b)

drops to about 1/8 in T7. Associated with this coarsening is an increase in more bulky, defected and less plate-like particles, presumably of Type 2 and/or η. These particles have not been investigated. Figure 1 shows examples of the two plate-shaped precipitate types in the two tempers in $\langle 112 \rangle$ Al projections. The plates are seen from the side illustrating that the plate normal always coincides with a $\langle 111 \rangle$ Al direction. In the following, we usually refer to absolute directions and planes associated with a particular choice of precipitate orientation, as given by the overlaid coordinate system (Fig. 1b).

Figure 1 shows that in the $[11\bar{2}]$Al projection the two precipitate types incorporate layers of a rhombic unit with corners defined by the high-contrast (Zn) atomic columns, similar to the rhombohedral (R) Zn units in η-MgZn$_2$ [11], which contain two Mg atoms. We define the precipitates as consisting of a *core* or an *inner* part plus a pair of interface planes (outer A-planes in Fig. 1a, b). The inner planes of the precipitates are denoted by the arrows on the left side in Fig. 1a, b. An R-layer has three atomic planes of two different types (dashed and solid arrow). The subsequent figures show higher detail. The core of Type 1 (Fig. 1a) consists of one R-layer together with a second layer built from orthorhombic (O) units, while Type 2 (variants) are

characterised by four R-layers in various stacking orders. Characteristic for the O-unit of Type 1 is a unique central atomic plane (*dotted* arrow in Fig. 1a). The two precipitate types have identical interfaces: Firstly, the top/bottom planes of a layer facing the matrix (corresponding to the outer solid arrows on the left side of the precipitates; see Fig. 1a, b) are identical. Secondly, the planes immediately outside are identical. They may be defined as solute-enriched Al planes, indicated with solid lines on the right side, and the letter 'A' in Fig. 1a. Although compositionally they belong to the precipitates, they are structurally more similar to (111)Al planes.

The ABC stacking of the (111)Al planes is indicated by letters and by the solid, dashed and dotted lines on the right hand side of the precipitates (Fig. 1a, b). They start/ end with the same plane (A), which implies an orthorhombic unit cell across the precipitate may be defined (as was used for the calculations). While in Type 1 five *inner* atomic planes always replace five (111)Al planes, in Type 2 nine such planes substitute eight (111)Al planes. This means the observed widths (including the interface planes) are nearly $6d_{111}^{Al}$ and $9d_{111}^{Al}$, respectively (Fig. 1a, b). Thicker Type 2 precipitates have also been found as demonstrated below. Figure 1 shows that a multitude of

unit cells may be defined which extend across the thickness, but repeat only in the plate plane. For first-principles calculations, the cells are integrated with the matrix. The threefold nature of the precipitates and Al-planes meant that the cells could be defined in space group $P3$. It was found convenient to let the unit cells start and end between planes and include equal amounts of Al-planes on each side. Let

$$a = a_l = a_0 + l d_{111}^{Al} \qquad (2)$$

so that $l \in 2Z$ (Z Al planes on each side). Then, a_0 is d_{111}^{Al} larger than the plate thickness (the observed distance between the outer A-planes), and $a_0^{Type1} \sim 7 d_{111}^{Al}$ and $a_0^{Type2} \sim 10 d_{111}^{Al}$. First-principles calculations used $l = 8$. Parameters of type a_8 are indicated in Fig. 1c, d.

Structure of the largest plates (Type 2)

The analysis begins with the thickest plates, as they are built by one type of layer.

Figure 2 is a cut-out across the plate in Fig. 1b, magnified and accompanied with an atomic structure model map. The elements and positions suggested fit intensities quite well. The interatomic distances vary little, and have normal values. The Zn-rich columns in the precipitate and Al columns in the matrix are easily identified in the image. The small dotted black rectangular overlay on the image traces out the η-cell. Atomic details can be compared with the 3D representation on the lower right. When consisting of at least two layers with the same orientation the rhombohedron may be defined as the unit cell of the (inner) precipitate.

The similarity with the η-phase suggests that some Zn columns should have twice the number of Zn atoms as the dimmer Zn columns. This correlates well with the two strongest contrasts in the image. A de-convolution [24] of the image in Fig. 1b was performed to enable a more detailed quantification of the columns. The results are summarized in Fig. 3. Together with a careful analysis of Fig. 2 and previous published work, the following conclusions emerged:

– The R-unit of the layers of Type 2 precipitates is isostructural with the rhombohedron in the equilibrium η phase, where two R-units define unit cell. It is realized as a rhomb in the [100] η projection. The lower right-hand side of Fig. 2 is a 3D perspective showing the zigzag stacking of this unit in the η-phase. The orientation of the R-units as observed here corresponds to the following orientation relation between the η-phase and aluminium:

$$(001)\eta \parallel (111)\text{Al}, \; [100]\eta \parallel [11\bar{2}]\text{Al}, \; [120]\eta \parallel [\bar{1}10]\text{Al} \qquad (3)$$

This is one of the frequently reported coherency relations of η [4]. In fact, when neighbour R-layers are mutually rotated 180°, appearing in a zigzag manner (η-like), the Type 2 and the η phase are isostructural, when neglecting the solute-enriched (111)Al interface planes (denoted 'A' in the figures).

– An interface between Type 2 and the matrix may be defined by three planes; (i) a pure (111) (matrix) Al plane (B), (ii) a solute-enriched Al matrix plane (A) which is split in two slightly separated subplanes of Zn and Mg and (iii) a Zn-rich (X) plane (top/bottom of an R unit in the η-phase equal to the top/bottom plane marked 'X' in Fig. 2). Along the [111]Al direction the precipitate consists of two different, alternating Zn-containing planes (XY…). The stacking of the Al matrix involves three planes (ABC…). From Figs. 1b and 2, it is seen that both the solute-enriched (111)Al planes (on opposite plate sides) next to the X layers are of type A.

– Regardless of the stacking order of the layers the rhombohedra appear with the same connection to the matrix at the main plate interfaces.

– The above discussion does not consider incorporation of Cu or Al within the structure or a Cu-enrichment in the (111)Al interface planes. The composition of precipitates in the peak hardness condition (T6) of the same alloy as used in the present paper has previously been investigated by APT [16], where an average of 7 % Cu and 18 % Al was found. Since Type 2 precipitates can be explained structurally in terms of the equilibrium η-phase, and since the presumed Mg positions appear with weak contrast, the Cu and Al are likely to replace Zn sites. See the discussion about composition below.

We can note that the variation in stacking of R-layers which define a Type 2 variant is quite analogous to how polytypes of Laves phases are described [12].

– From Fig. 2 it can be seen that the interface periodicity along the $[\bar{1}10]$Al direction is 904 pm according to the η-phase, while 858 pm in Al. This corresponds to a mismatch of 5.1 %. However, it should not be expected that the cell parameters of large single crystals of η-would be identical to the very fine coherent precipitates inside the matrix, even if the atom types were identical. Partial replacements of Zn by Cu and Al in the precipitates and in the enriched (111)Al interface planes could further affect the mismatch.

– From the direct HAADF-STEM observations and the intensity profiles (Fig. 3c), it can be inferred that the Al columns forming the solute-enriched (111)Al planes (at both sides of the plate) are either fully or partly replaced by Zn and Mg with alternating Zn–Zn–Mg–

Fig. 2 Central part of Type 2 (of Fig. 1b). Heights and distances on atomic map (*right*) and in legend correspond to the initial model *before* first-principles refinements. Three lower (*yellow*) overlaid rhombs show the η-like stacking (RR^{-1}) and two upper (*pink*) rhombs the stacking (RR). *Dotted black rectangle* traces η unit cell along [100]η. ABC and XY refer to (different) stackings of Al and precipitate planes. Distance between *double lines* indicates periodicity along [$\bar{1}$10]Al of Al and η. Projected inter-columnar distances have grey background. *Large stippled rectangle* Orthorhombic cell with two matrix (111)Al planes ($a = a_2 \sim 12d_{111}^{Al}$). Refinements included four planes on each side ($a = a_8$). *Lower right* Perspective of η with building R-units. Central unit (R^{-1}) is rotated 180° relative to R. See previous figure (Color figure online)
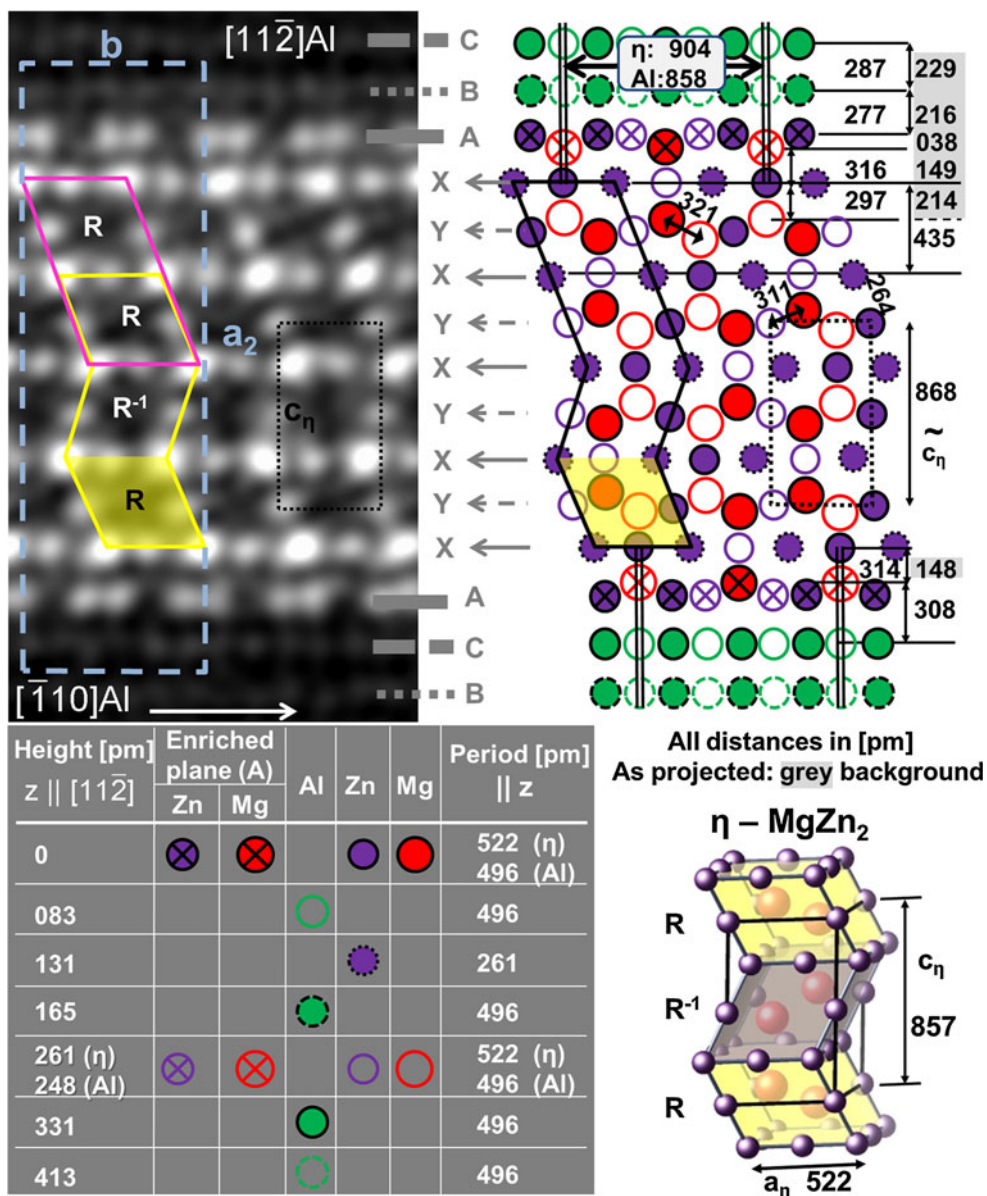
Zn–Zn columns along [$\bar{1}$10]Al (Fig. 2). Assuming that the brightest contrasts are columns with pure Zn, and the lower contrast columns of the same plane are Mg, the enriched matrix layer can be viewed as split into two elemental planes (Fig. 4). By the principle of minimum atomic separation with regard to the atomic radii in the elemental phases, from the initial model it was inferred that the plane holding the Mg atoms (large, red circles in Fig. 4d) has separation approximately 178 pm from the precipitate X-plane. The model sets the real distance from such Mg atoms to the nearest Zn atom in the X-plane to 316 pm. A second plane holds the Zn atoms and was modelled to be about 216 pm from the X-plane. The smallest distance between Zn atoms of this plane and those of

the X-layer is 263 pm. The separation between the two layers (c.f. Fig. 2) could then be estimated to be about 40 pm. From the HAADF image analyses (Fig. 3c), a split could be confirmed. Here, the projected distances from the X-plane to the two split planes were found to be slightly larger than expected, being 200 pm for the Mg-rich plane and 230 pm for the Zn-rich plane, which sets the separation to about 30 pm. This observation might imply that the Al atoms in the enriched (111)Al plane adjacent to the precipitate X-plane are only partly replaced by Zn and Mg. A thin Al-layer above/beneath the specimen will have the same effect; the contribution from matrix Al atoms of normal (non-split) planes will bring the Zn and Mg peaks closer together, underestimating the split.

Fig. 3 a Intensity profiling of Type 2 variant in Fig. 1d. Three elongated rectangles exemplify regions of profiling, **b** average of 13 profiles in direction 1 (long diagonal of rhombs) shows peaks corresponding to expected Zn and Mg columns of the η-type rhombohedron (c.f. text and Fig. 2), as indicated in the rhombic cell overlay, **c** average of 13 intensity profiles across the matrix enriched (interface) plane, indicating it is split into Zn and Mg subplanes. Profile in rectangle 3 crosses the atomic columns rich in Zn, whereas profile 2 crosses the column which is likely to be occupied by Mg atoms
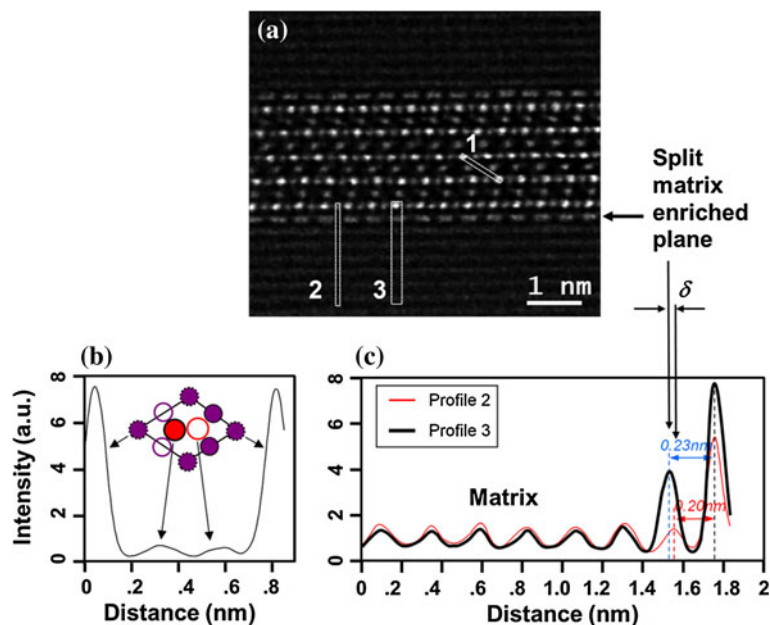
For the first-principles refinements of the Type 2 precipitates, initial orthogonal super-cells of dimension $a = a_8 = 4.198$ nm, $b = 0.904$ nm and $c = 0.522$ nm were used. They correspond to an augmentation of the large stippled rectangle in Fig. 2 (where $a = a_2$), but with six more (111)Al planes. See Fig. 1 for overview. Parameters b and $c = b/2\cos(30)$ are chosen to correspond to the hexagonal plane periodicity in η.

The initial cells, which were adjusted to fit the (R-layers of the) equilibrium η phase, shrank towards more Al-like volumes. For example, the cell related to Fig. 2 went from 1.98 to 1.87 nm³, as compared with 1.80 nm³ for the super-cell in Al; the parameters changed to 4.16 nm ($18d_{111}^{Al} = 4.208$ nm), $b = 0.885$ nm ($6d_{220}^{Al} = 0.86$ nm) and $c = 0.509$ nm ($6d_{224}^{Al} = 0.496$ nm). The separation between the X and Y layers of the rhombic unit remained constant (0.214 nm). The projected separation at the coherent interface between the Mg columns in the enriched Al layer and the X-plane was refined to 0.169 nm, and the projected distance between the Zn columns of the same layer to the X-plane was refined to 0.227 nm, which means the split refined to $\delta = 58$ pm. As explained above, the discrepancy between this refined separation and the estimated (~ 30 pm) value from the intensity profile scans of the HAADF image (Fig. 3c)—is probably due to an Al component in the split layers.

Crystal structure of Type 1 precipitates

Images like Fig. 1a strongly indicate that Type 1 precipitates connect in the same way to the Al matrix as Type 2, and that also this structure incorporates the R-unit of the

equilibrium η phase. The difference between Type 1 and 2 is that Type 2 normally comprises four R-layers stacked in different ways (Figs. 1b, d, 2), while Type 1 only contains one R-layer together with an orthorhombic (O) layer, as denoted in Fig. 1a. Based on the Z-contrast information in the HAADF-STEM image in Fig. 1a, on the number and location of various atomic columns, on calculated interatomic distances and on the expectation of a dense packing, two different models for the Type 1 precipitate could be proposed. In Fig. 5a, b, the models are shown *after* the respective first-principles (VASP) refinements were performed. They correspond to the low enthalpy configurations types 1a_ZnMg and 1b_ZnMg (see the VASP part below and Table 1). The following observations were made:

– In the first-principles refinements of Type 1, orthogonal super-cells were used, having dimensions $a = 3.507$ nm, $b = 0.904$ nm and $c = 0.522$ nm for the model in Fig. 5a, and $a = 3.477$ nm, $b = 0.868$ nm and $c = 0.501$ nm for the model in Fig. 5b. The cells both correspond to the large stippled rectangle in Fig. 5 ($a = a_2$) plus six more (111)Al planes ($a = a_8$). Because of the R-units, the cell dimensions in the (111)Al plane were implicitly increased to match those of η-MgZn$_2$. The periodicity along $[\bar{1}10]$Al, which can be compared with $6d_{220}^{Al} = 0.859$ nm) refined to 0.884 nm (~ 2 % decrease) and to 0.875 nm (~ 1 % increase) for the models in Fig. 5a, b, respectively. The periodicity along $[11\bar{2}]$Al, which can be compared with $6d_{224}^{Al}$ (0.496 nm) refined to 0.501 and 0.500 nm for the same two models. Here, the parameter for model 1a shrank 4 %, while for 1b it was left unchanged. Since in any case, both dimensions
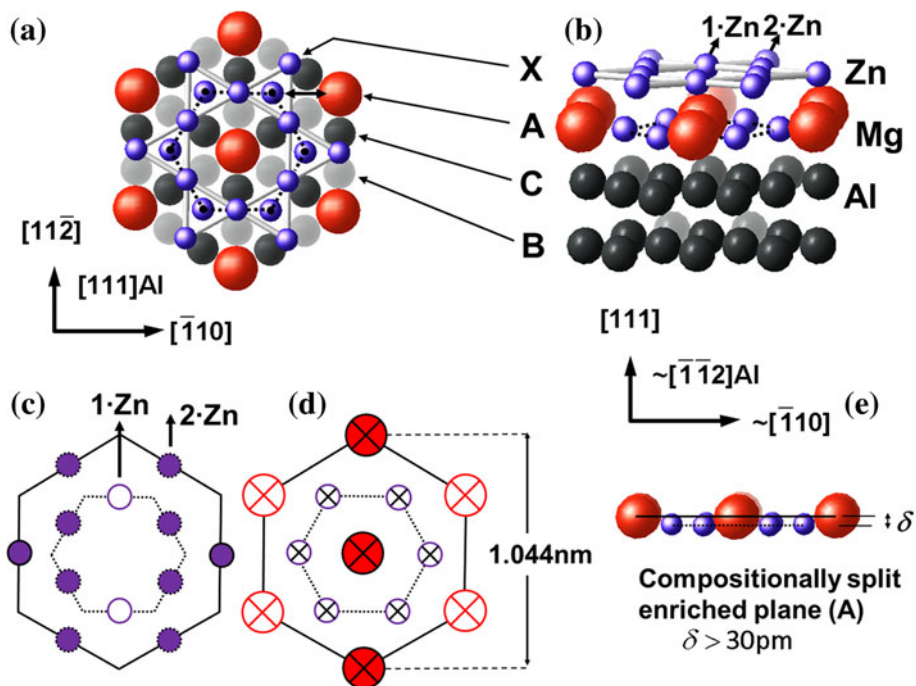
Fig. 4 Reconstruction of (model) interface region for both precipitate types (lower parts of stippled unit cells in Figs. 2 and 5). *Letters A, B and C* denote planes of the normal (ABC) fcc Al stacking. Zn-atoms in plane A are connected by a *black, dotted hexagon*. X is one of two types of precipitate planes (see Fig. 2). **a** [111] Al projection of the two outermost Zn-containing planes plus two Al planes, **b** the same planes near $[11\bar{2}]$Al, (**c**, **d**) planes X and A, respectively, in [111]Al projection with symbols representing atomic heights along $[11\bar{2}]$Al (c.f. legend in Fig. 2), where superposed hexagons coincide in projection, **e** Mg and Zn atoms in the Al-type interface plane (A) splits into two planes with separation $\delta = 30$–60 pm (confer Figs. 2, 3c). Scale (**d**) is based on the hexagonal η-MgZn$_2$ phase. The Mg- and Zn-planes [large/small hexagons in (**d**)] refined to 169 and 227 pm from X, respectively. In X, columns with single and double number of Zn-atoms along $[11\bar{2}]$Al are shown. In (**a**, **b**), these atoms are connected by *thick white lines* (Color figure online)

exceed those of the Al super-cell, this indicates that an expansive strain will surround the plate in the radial direction. The cell parameter along the plate normal reduced to 3.408 nm (~ 3 %) and 3.436 nm (~ 1 %) for the models in Fig. 5a, b, respectively, well below the super-cell in Al ($15d_{111}^{Al} = 3.507$ nm). This is an indication of contractive strain in the surrounding Al matrix, along [111]Al.

– The Type 1a model in Fig. 5a has a better fit with the experimental image as compared to the Type 1b model in Fig. 5b. In particular, the Zn columns in the lower X-layer of Type 1b, initially forming a straight line along $[\bar{1}10]$Al, refined to positions resulting in a wavy appearance, which is not observed in the HAADF-STEM images. The middle X-layer of Type 1b is also wavy. The distortion of the two X-layers modifies the geometry of the R-unit. No significant perturbations of the X-layers or the R-units were observed with the refinement of Type 1a.

– With some justification, both the R- and the O-units can be viewed as super-cells in the Al matrix, as indicated in Fig. 5c. We can see this by (i) the merging of two Al columns (indicated with dotted ovals in Fig. 5c) into one column with twice the occupancy, corresponding to the densest Zn columns at the corners of the units, and (ii) change in atomic height z (along $[11\bar{2}]$). The Type 1b model contains the same number of atomic columns as the Al super-cells, while Type 1a has an extra column that would correspond to a split of every third column of the middle layer of the orthorhombic super-cell (that corresponds to the A′ layer in the Type 1 precipitates) into two columns. According to the VASP calculations and Z-contrast information in the HAADF-STEM images (see the following paragraph), the A′ layer in Type 1 precipitates most likely consists of Mg and Zn atomic columns, as sketched in Fig. 5a, b. Plane A′ is marked as such due to the atom heights, which correspond to the layer A in the aluminium (see Fig. 5 and the legends of Figs. 2, 5).

– The interatomic distances between the Mg atoms in layer A′ were refined by VASP to 290–292 pm and 284–291 pm for the Type 1 models presented in Figs. 5a, b, respectively. These are shorter than 320 pm, the respective distance in elemental Mg and in the equilibrium η-phase. This may be a sign of partial replacements of these columns by Al.

Fig. 5 Magnified part of the Type 1 precipitate in Fig. 1a. Atomic structure maps (**a**, **b**) correspond to two low enthalpy models *after* refinements (p and q denote Zn and Mg). Legend supplements that of Fig. 2, with initial model measures. Projected distances have grey background. The interface with the aluminium (Fig. 4) is identical for both types. Type 1 consists of one layer of R-units [projected to a rhomb with light (*yellow*) fill] and one layer of orthorhombic (O) units (rectangular projections). **c** [11$\bar{2}$]Al projection showing that in the Al matrix super-cells for both R and O may be assigned. They are realised by merging each of the two columns indicated by the *dotted ovals* into one corner column (which doubles the occupancy) and re-arranging the heights of the remaining columns such that the stacking sequence changes from ABC (Al) to XY (precipitate). Large stippled rectangle: Orthorhombic cell with two (111)Al planes ($a = a_2 \sim 9d_{111}^{Al}$). Refinements had eight external planes ($a = a_8$). See Figs. 1 and 2 (Color figure online)
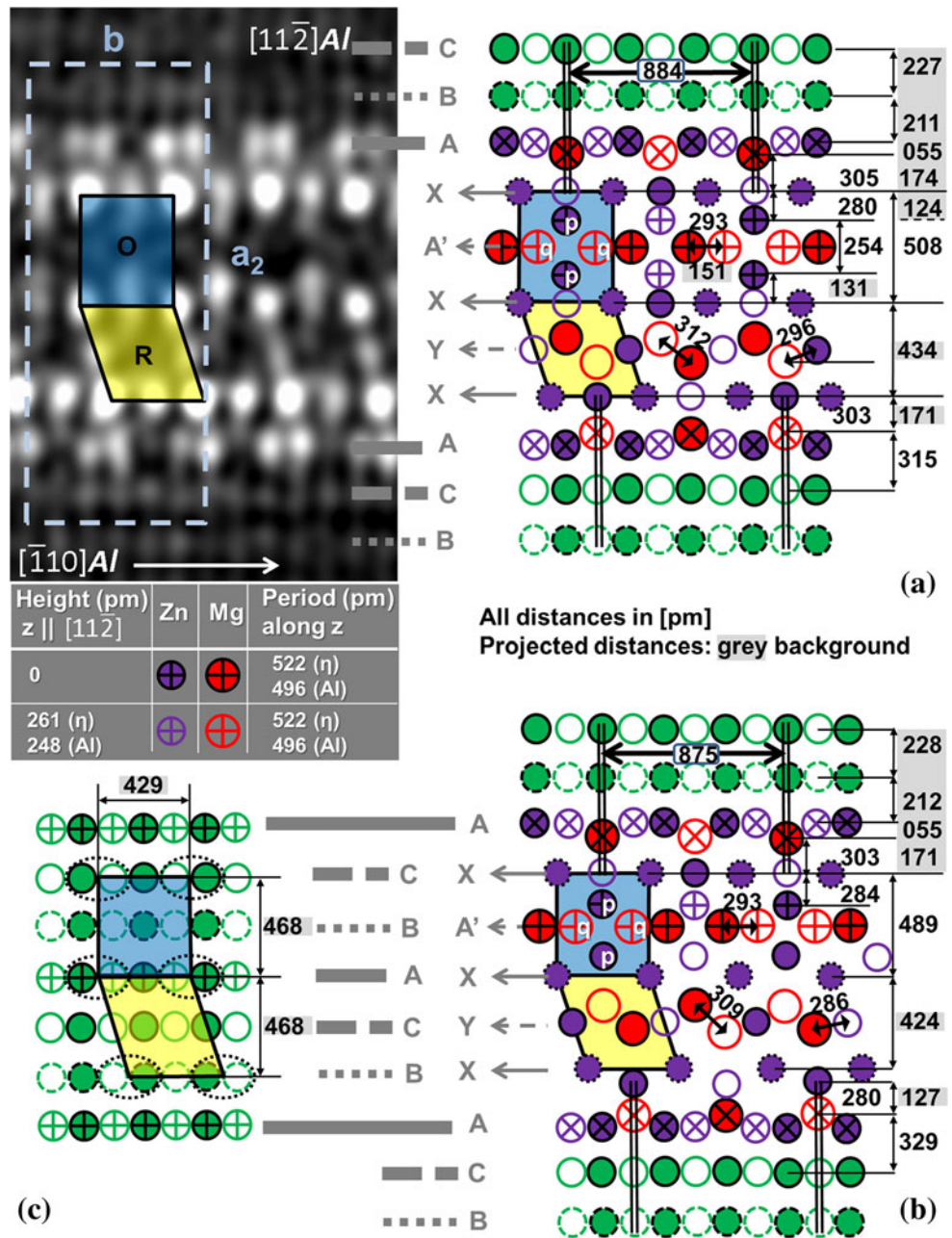
First-principles calculations

As discussed, eight external Al planes were chosen for the refinements. It was required that the number of such planes be 2, 5, 8, …, $n + 3$; i.e. super-cells with cell parameters a_2, a_5, a_8, …a_{n+3} across the precipitate should be used. Only these choices can prevent stacking faults in the (periodically generated) Al-slabs between the precipitate cores in the [111]Al direction. This may be understood in the following way: Referring to the inner particle (core) in Fig. 2 as 'P' and to the split interface layer of type A as 'α',

from bottom and up the supercell a_8 (which includes the external planes B and C) may be written as $a_8 = C[\alpha P\alpha]B$. This creates the smallest possible stacking fault free series; $a_2 a_2 \ldots = C[\alpha P\alpha]BC[\alpha P\alpha]C\ldots$. It is easy to see that the central stacking-free Al-slab can only be achieved by adding triples of layers (ABC) in between every two cells (after each 'C'). This applies for Type 1 as well, as is clear from Fig. 5.

Two Type 1 models are shown in Fig. 5a, b. They correspond to low enthalpy configurations after the first-principles refinements. The refinements concern coordinates,

but it was also checked for type of element. This was necessary as the Z-contrast information in the HAADF-STEM image and inter-atomic distances did not lead to one unambiguous conclusion. The formation enthalpies for all investigated structures are presented in Table 1. The Type 1 models are labelled as Type 1x_pq. Here, x is either a or b, corresponding to the two models shown in Fig. 5a, b, respectively. The letters 'p' and 'q' refers to type of atom at the, respectively, marked sites in Figs. 5a, b. Two models of Type 2 precipitates were investigated: Type 2_η corresponds to the η-like stacking with four R-units zigzagging across the width (RR^{-1}RR^{-1}), while Type 2 corresponds to the more general, less symmetrical model presented in Fig. 2, with stacking RRR^{-1}R. Here, R^{-1} designates 180° rotation of the R-layer or a single R-unit. The described perfect η-like stacking (Type 2_η) was observed in lower amounts (see Fig. 6b as example). For comparison, a VASP refinement was also performed on the bulk η structure [11].

The formation enthalpies were calculated as

$$\Delta H = E_{tot} - E_{matrix} - n_{Al}E_{Al} - n_{Mg}E_{Mg} - n_{Zn}E_{Zn} \qquad (3)$$

where E_{tot} is the total enthalpy of the calculation cell after relaxation, E_{matrix} the enthalpy corresponding to the matrix Al atoms included in the calculation cell for Type 1 and Type 2 precipitates, n_X the number of atoms of type X in the precipitate and E_X the enthalpy of an atom type X in solid solution.

For Type 1 and Type 2, the values of E_{matrix} were obtained from bulk calculations of slabs with 48 Al atoms strained in the same way as the matrix atoms in the super-cells. For pure η, E_{matrix} is zero. The values of E_X were obtained as the enthalpy of a face centred cubic (fcc) super-cell with 255 Al atoms and one solute atom X, minus 255

times the mean Al enthalpy in a corresponding super-cell with 256 Al atoms. Hence,

$$E_X = E_{Al255X} - \frac{255}{256}E_{Al256}. \qquad (4)$$

From Table 1, the following can be concluded:

– The stable η-phase has the lowest formation enthalpy, followed by Type 2 again which have lower formation enthalpies than Type 1.

– Type 1a has on average lower formation enthalpies than Type 1b.

– For Type 1a, the lowest formation enthalpies concern two configurations: one, corresponding to Mg occupying both sites p and q, and the other with Zn on site p and Mg on site q in the orthorhombic unit cell. Type 1b has the lowest formation enthalpy with Zn on site p and Mg on site q. Based on these observations and on the Z-contrast information provided by the HAADF-STEM images, we regard the most likely configurations for the Type 1 precipitates as 1a_ZnMg and 1b_ZnMg, shown in Fig. 5a, b, respectively.

– There is negligible enthalpy difference between the two Type 2 structures, indicating no enthalpy gain for choosing one stacking variant (say RR^{-1}RR^{-1}) over the other (RRR^{-1}R). This implies a low enthalpy exists for the R-layer (or unit), and it strengthens the observation that the concept of R-layers represents the Type 2 precipitates quite well.

The orthogonal cells used for the calculations of the Type 1 and 2 models were set up as super-cells in the Al matrix, as indicated by the stippled rectangle overlays in Figs. 2 and 5, which include Al-layers on both sides. All the calculations were performed without restrictions
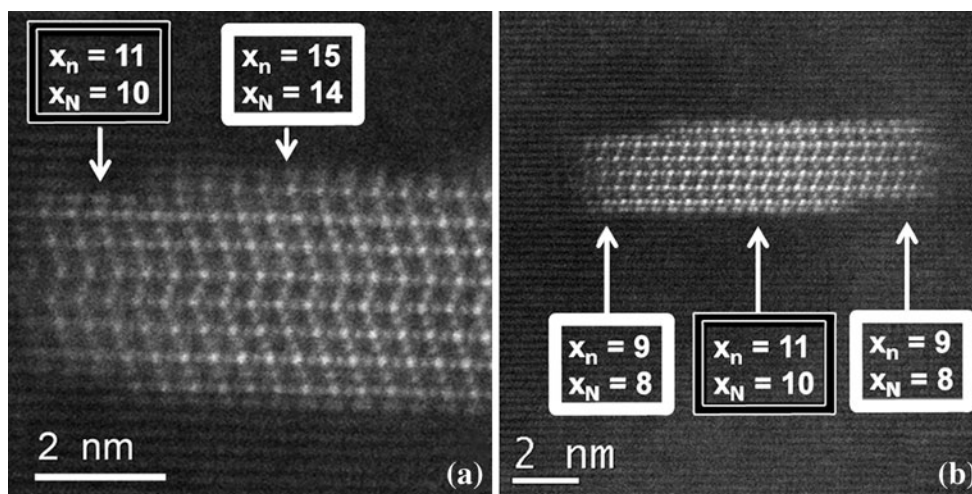
Fig. 6 HAADF-STEM images of Type 2 precipitates not adhering to the rule of mismatch minimization (Table 3). The precipitates have the same crystallographic orientations as in Fig. 1. The precipitates in **a** and **b** indicate a stepwise growth with parts fulfilling the rule (*white boxes*), and parts which do not (*black boxes*). The precipitate in **b** has a perfect η-type stacking (RR^{-1}RR^{-1}...)

regarding symmetry (space group $P1$). However, the atoms in all the precipitate planes have threefold ordering. The layers of rhombohedra relate to the high hexagonal symmetry of the η-phase [$P6_3$/mmc (194)]. Although the alternative stacking [Type 2 instead of Type 2_η (Fig. 2)] breaks elements of this symmetry, the penalty is low (Table 1), which means that keeping the atoms in (layers of) η type rhombohedra is much more important than the stacking sequence of the layers. It should be expected that the overall lowest enthalpy complies with the highest symmetry. It was therefore investigated whether any of the refined structures could be described in higher symmetry, i.e. if a unit cell could be found, which would include both precipitate and matrix, in a higher symmetry than $P1$. It was found that unit cells and atomic coordinates of the Type 1a and both Type 2 structures fit well space group $P3$ (143), even for arbitrary numbers of Al planes (See Fig. 1 and Eq. 1). In Table 1 are given the refined orthorhombic unit cell parameters for eight added planes ($a = a_8$). In Table 2 we provide also the coordinates in $P3$ of Type 1a_ZnMg and Type 2, with one Al layer on each plate side. (The Type 2 variant has the stacking different from η). Cells and coordinate data of the trigonal space group were extracted from the refinements of the orthogonal ($P1$) cells. Cell parameters and coordinates had to be averaged or approximated with some loss of accuracy, but in this form the data enables much easier inspection of the structures. For future calculations, extended cells can be based on the structure data as given in Table 2, provided a sufficient number of Al-layers are added. Note that the rhombohedral axis (c-parameter) now coincides with previous choices for the a-axis (along the plate normal); $c = a_2$. The large stippled rectangle overlays on the images in Figs. 2 and 5 show the rectangular cells with size a_2 along [111]Al and b along [$\bar{1}$10]Al. The trigonal cell in Table 2 would in this projection be a rectangle with similar height ($c = a_2$), but half the width ($b/2$).

Precipitate transversal growth

It was investigated whether the layer stability and the precipitate interface connections with the Al matrix through the X-planes represent limiting factors regarding the thickness of the plates: As already noted, the inner part of Type 1 precipitates contain five planes (XYXA′X), while Type 2 contains nine planes (XYX…X). Referring to Fig. 1a and the specific stacking in Fig. 1c, recalling that the rhombohedral and orthorhombic units could be defined as XYX and XA′X, respectively, the five and nine planes could be designated RO and RRR^{-1}R. Due to the small energy difference between the various stacking, it should be expected that the

Table 2 Refined cell parameters and coordinates in space group $P3$ (143), of low enthalpy models of the two precipitate types, including interface and two external (111) Al-planes (c equals the a_2 shown in Figs. 2 and 5)

Type 1a_ZnMg				Type 2 (η-polytype shown in Fig. 2)			
$a = b = 0.506$ nm, $c = 2.049$ nm				$a = b = 0.51$ nm, $c = 2.811$ nm			
Atom	X	Y	z	Atom	x	Y	z
Zn 1	0	0	0.1582	Zn 1	0	0	0.1194
Zn 2	0	0	0.8418	Zn 2	2/3	1/3	0.1194
Zn 3	1/3	2/3	0.1582	Zn 3	1/3	1/6	0.2000
Zn 4	2/3	1/3	0.8418	Zn 4	2/3	1/3	0.2764
Zn 5	0	0	0.3768	Zn 5	1/2	0	0.3525
Zn 6	1/3	2/3	0.5466	Zn 6	2/3	1/3	0.4287
Zn 7	1/3	2/3	0.6703	Zn 7	1/3	1/6	0.5000
Zn 8	1/6	1/3	0.2703	Zn 8	2/3	1/3	0.5713
Zn 9	1/3	1/6	0.4831	Zn 9	1/2	0	0.6475
Zn 10	5/6	1/6	0.7297	Zn 10	1/3	2/3	0.7237
Mg 1	2/3	1/3	0.1858	Zn 11	1/6	1/3	0.8000
Mg 2	1/3	2/3	0.8142	Zn 12	1/3	2/3	0.8806
Mg 3	2/3	1/3	0.6068	Zn 13	0	0	0.8806
Mg 4	2/3	1/3	0.3481	Mg 1	1/3	2/3	0.1398
Mg 5	0	0	0.6068	Mg 2	1/3	2/3	0.2552
Mg 6	1/3	2/3	0.4034	Mg 3	0	0	0.2958
Al 1	1/3	1/3	0.0556	Mg 4	0	0	0.4090
Al 2	0	1/3	0.9444	Mg 5	1/3	2/3	0.4482
				Mg 6	1/3	2/3	0.5518
				Mg 7	0	0	0.5910
				Mg 8	0	0	0.7042
				Mg 9	2/3	1/3	0.7448
				Mg 10	2/3	1/3	0.8602
				Al 1	1/3	1/3	0.0452
				Al 2	1/3	0	0.9548

Data are extracted from the refinements with orthogonal ($P1$) cells with 8 external Al-planes (a_8). Structures correspond to particles in Fig. 1a, b

thickness of the plates is controlled by the number of such units. Therefore, to extend the thickness, in principle a pairwise increase in precipitate planes is expected, the pairs being either YX or A′X. However, as shown below, this also depends on the number of Al (111) planes.

From Figs. 2 and 5 it can be seen that the plate thickness of Type 1 and 2 precipitates requires that the number of precipitate planes matches a number of Al planes in a way that the terminal X-layers face the solute-enriched (A) Al layers with the same heights on both precipitate interfaces (Figs. 1, 2, 5). This should correlate with minimum mismatch. In the case of Type 2 precipitates, the distance between X and Y layers is 214 pm (derived from the

dimensions of η and also left unchanged by the VASP refinements). The (111)Al plane distance is 234 pm. Based on the above requirements it may be concluded that the smallest Type 2 precipitate thickness will consist of 5 planes (XYXYX) matching the same number of Al planes (BCABC). Therefore, the Type 2 plate thickness should be restricted to the following number of planes: $x_n = 5 + 2n$, $n = 0, 1, 2…$, while the number of displaced Al planes becomes $x_N = 5 + 3N$, $N = 0, 1, 2…$ Thus, the corresponding mismatch along the plate normal will be minimized when the following expression approaches zero:

$$M_{\text{Type2}} = \frac{214(x_n - 1) - 234(x_N - 1)}{234(x_N - 1)} \quad (5)$$

Table 3 shows calculations of the mismatch between the x_n precipitate planes and the displaced x_N Al planes along the transversal growth directions parallel to [111]Al.

For Type 1 precipitates, the mismatch was calculated for the lowest enthalpy configurations shown in Fig. 5a, b by taking into consideration the VASP refined dimensions of the R- and O-units:

$$M_{\text{Type1a\_ZnMg}} = \frac{(526 + 439) - 234(5 - 1)}{234(5 - 1)}$$
$$= +0.0456(4.6\%) \quad (7)$$

$$M_{\text{Type1b\_ZnMg}} = \frac{(507 + 440) - 234(5 - 1)}{234(5 - 1)}$$
$$= +0.0118(1.2\%) \quad (7)$$

It was found that all the experimentally observed precipitates have a misfit $M < 5\%$. It should be noted that the (two) enriched interface planes are external to the O and R units and are counted as Al planes. This is justified by the line profile measurements shown in Fig. 3 and the VASP refinements indicating the corresponding spacing (the average separation between the enriched Al planes and

Table 3 Estimated and observed (core) plate thickness for Type 1 and 2 precipitates (see Fig. 1), based on respective numbers 17 and 26

Number of planes in η	Replaced Al (111) planes	Mismatch (%)	Encountered plate thicknesses	
$x_n = 5 + 2n$	$x_N = 5 + 3N$	Along [111]	Type 1	Type 2
5	5	−8.4	–	NO
5	5	+1.2 to +4.6	O[a]	–
7	5	+37.3	–	NO
9	8	+4.6	–	O[a]
13	11	+9.9	–	NO
15	14	−1.4	–	O
19	17	+3.0	–	NO

Observed/not observed (O/NO)

[a] Plate structures described in this work

the adjacent precipitate interface X-plane) is close to the (111)Al lattice spacing.

The reason the thicker Type 2 precipitates of the last row of Table 3 (3 % mismatch) have not been observed, may be that higher temperatures and/or longer heat treatment times would be required. Higher temperature should produce the less coherent equilibrium phase η-MgZn$_2$. In principle, this phase would be independent of the matrix and controlled only by the number of rhombohedra.

Figure 6 shows that some precipitates have step-like cross sections with (larger) thicknesses that appear not to adhere to the above growth scheme (Table 3). Still, the particle interfaces are clearly highly coherent. In Fig. 6a, the misfit occurs near the plate edges, which may indicate it is in a state of growth (or shrinkage). The particle in Fig. 6b gives an impression of having been sheared. It is also possible this symmetry could be created by a merging of two smaller parallel precipitates, which are centred about different Al (111) planes. It is not investigated whether heterogeneous nucleation on a dislocation or some stacking fault in the aluminium may be behind such deviations.

Discussion

The results support the findings of Li et al. [23], where aberration corrected HAADF-STEM was used for a similar alloy. While in the present work the precipitates were investigated with the matrix oriented in a $\langle 112 \rangle$ Al zone, they based their analyses on images taken in $\langle 110 \rangle$ Al projections. The current results match and extend the previous results [23] and are therefore discussed in conjunction:

– Most precipitates are comprised by 5 and 9 atomic planes replacing 5 and 8 {111}Al planes, respectively, plus two external solute-enriched (Al) planes. In Ref. [23], the 5-plane precipitates were categorised as Types I, II and III, and were identified as η', while the 9 plane precipitates were identified as η. The main differences between these types were their extent in the {111}Al habit planes and the apparent stacking of planes as ABC (matrix) or ABAB. The present work shows that it is very likely that all plate precipitates with thickness spanning five {111}Al planes are of the same type (here called Type 1), and have an overall appearance as shown in Figs. 1a, c and 5. This conclusion is backed by a number of recorded images of precipitates having this thickness, but with variable plate diameters in the {111}Al habit plane (not shown in this paper). A word of caution for the smallest diameters: The precise stacking of layers in small Type 1 precipitates is not always easy to identify (c.f. Fig. 1c) as there is usually more overlap with the Al matrix along the viewing direction.

– The current investigations also confirm the noted lack of observations in Li et al. [23], regarding precipitates with crystal structures resembling any of the previously published models of η'. Instead, the two types of coherent, fine plate-shaped precipitates addressed here contain layers of similar R-units that can be derived from the structure of the equilibrium η phase. However, we cannot completely exclude the possibility that the Cu content has some influence on the precipitate structures although in the case of Cu-free alloys, one probably should expect even less deviation from the equilibrium phase geometry.

It is clear that the precipitates in the investigated alloy may be described as layered structures, and that they contain similar or the same layers in various stacking formations. The main difference between the two precipitate types is clearly the different orthorhombic type of layer only contained in Type 1 (Fig. 5). Since the two different layers are themselves connected through a common atomic plane, this implies that both layers (because of symmetry) face the matrix with similar atomic configuration, which may be viewed as an argument for the similar connection of the two units with the matrix. The proposed atomic models are well supported by the VASP calculations (Table 1); Type 2 precipitates have formation enthalpies comparable to the equilibrium η-phase. Virtually no enthalpy difference has been found between variants with differently stacked R-layers. This indicates high stability for the layers, and higher probability for stacking disorders. Type 1 precipitates have slightly higher formation enthalpy as compared to Type 2, which may indicate this phase can form at lower temperatures (or earlier in the precipitation sequence) and has a better coherency with the matrix. The trend of decreasing formation enthalpies for phases in the precipitation sequence when 'moving towards' the equilibrium phase has also been reported in the Al–Mg–Si (6xxx) system [28].

It should be noted that the described precipitates have no periodicity along the plate normal. Thus, the unit cell parameters can be well defined in the plate plane, but that the choice of cell parameter normal to the plate is generally arbitrary as long as it surpasses the plate thickness. The precipitate is well integrated with the matrix (111) planes. A useful and complete description of the unit cell of such precipitates should therefore both include the atoms of the interface, as well as contain or show in detail how the (111)Al planes of the aluminium can be included.

In a recent publication [29], aberration corrected HAADF-STEM and phase retrieval from aberration corrected HRTEM images were used in combination with first-principles calculations to study the very fine T_1-plate precipitate in the Al–Li–Cu system, which also forms on {111}Al planes. Comparison of the T_1 model and the previously published HAADF-STEM images [29] with similar images for the plate precipitates in the present work showed a remarkable match in structure and intensity distribution with the O-layer of the Type 1a phase. In addition, the T_1 interface with the Al matrix, which is identical on the two sides, appears exactly as the presently investigated interfaces of Types 1 and 2. Comparing with the O-layer (Fig. 5), the strong intensity Zn-columns defining the corners of the O-unit in our models correspond to mixed columns of Al and Cu in Dwyer et al. [29]. There, the interior of the unit was defined as a central Li layer between two Al layers. The similarities with the present work indicate that Mg takes the role of Li while Zn acts like Al (see corresponding atomic sites p and q in Fig. 5a, b). Thus, the T_1 phase is most probably isostructural to the O-layer in Type 1a precipitates. It may therefore be expected that in some conditions a plate isostructural to the T_1 phase could also exist in the Al–Mg–Zn system. Time will show whether such a phase could exist, and whether any of these phases should be identified with GP-zones or η'.

The investigated alloy contains Cu. For the same alloy composition and T6 heat treatment, APT previously has shown that both Cu and Al are contained in the precipitates [16]. Based on the Z-contrast information in the HAADF-STEM images, the only atomic columns with sufficient intensity to account for appreciable amounts of Cu are those of Zn. That Cu occupies such positions makes strong sense in light of the Cu sites in the T_1 phase [29], together with the fact that Cu and Zn are neighbours in the periodic system. APT results have indicated that Cu is present in the core of the precipitates [15, 16] and is not segregated at the interfaces. Engdahl et al. [15] also showed that Zn defines a larger precipitate volume than Mg. This is consistent with the Zn-rich X-layers forming the interface of Types 1 and 2 precipitates, and with the assumption that Zn is present in the adjacent solute-enriched matrix layers.

The similar Z-contrast from neighbour elements makes discrimination in HAADF-STEM images between Mg and Al challenging. According to the analogy with the published T_1 phase [29], Al may define the atomic sites p in the A' layer of the orthorhombic unit of Type 1 precipitates, while Mg the sites q (Fig. 5). However, when judged by the intensity in the HAADF-STEM images and formation enthalpies (Table 1), we here find that the atomic sites p are most likely Zn and sites q are Mg, although shorter Mg–Mg inter-atomic distances may suggest mixed columns of Mg and Al.

A fraction of Zn may also be substituted by Al, which could apply to any Zn position. This is based on the observation that Zn can replace Al in the enriched Al layers

adjacent to the precipitate interface. Adding support is the suggested substitution of Cu by Al in analogue positions of the T_1 phase [29]. APT composition measurements of the metastable precipitates showing Zn/Mg ratios between 0.9 and 1.4, as compared to 2 in the equilibrium η-phase, indicate the same thing. Unfortunately, precise quantification of Al in the precipitates is difficult using APT. This is mainly due to atomic trajectory delocalisation—a consequence of the different evaporation rates of atoms in precipitates and in the Al lattice [3, 13, 15, 16, 19].

In any case, resolving the questions related to composition will probably require a combination of new, dedicated HAADF-STEM experiments together with first-principles calculations in an amount which has been outside the scope of this work.

Conclusions

In this paper, we demonstrate a strong structural link between the equilibrium η-$MgZn_2$ phase and precipitates in the Al–Mg–Zn–Cu system, and report the crystal structures of two coherent, metastable plate-shaped precipitates having main habit planes {111} Al. Both types incorporate layers of a rhombohedral (R) structural unit present also in the η-$MgZn_2$ Laves phase. Most Type 2 plates consist of four layers, stacked either pairwise parallel or relatively rotated 180° (η-like). Type 1 contains one R-layer together with an orthorhombic layer isostructural with the single layer T_1-phase of the Al–Li–Cu system. It is suggested that a similar phase may exist also in Al–Mg–Zn (–Cu) for some conditions. Atomic models were extracted from HAADF-STEM images and investigated by first-principles calculations. The two structures can be described in space group P3 together with any number $l = 2Z$ of external (111) Al planes. Unit cells and coordinates for $l = 2$, extracted from the calculations are given. Small enthalpy differences between Type 2 variants confirm stability of the R-layers. The width of Type 1 and the step-wise growth of Type 2 precipitate thickness have been explained by geometry and mismatch with the Al matrix.

References

1. Degischer HP, Lacom W, Zahra A, Zahra CY (1980) Z Metallk 71:231
2. Berg LK, Gjønnes J, Hansen V, Li XZ, Knutson-Wedel M, Waterloo G, Schryvers D, Wallenberg LR (2001) Acta Mater 49:3443
3. Sha G, Cerezo A (2004) Acta Mater 52:4503
4. Gjønnes J, Simensen CJ (1970) Acta Metall Sin 18:881
5. Auld JH, Cousland SM (1974) J Aust Inst Met 19:194
6. Li XZ, Hansen V, Gjønnes J, Wallenberg LR (1999) Acta Mater 47:2651
7. Kverneland A, Hansen V, Vincent R, Gjønnes K, Gjønnes J (2006) Ultramicroscopy 106:492
8. Kverneland A, Hansen V, Thorkildsen G, Larsen HB, Pattison P, Li XZ, Gjønnes J (2011) Mater Sci Eng A 528:880
9. Wolverton C (2001) Acta Mater 49:3129
10. Friauf JB (1927) Phys Rev 29:34
11. Komura Y, Tokunaga K (1980) Acta Cryst B 36:1548
12. Stein F, Palm M, Sauthoff G (2004) Intermetallics 12:713
13. Stiller K, Warren PJ, Hansen V, Angenete VJ, Gjønnes J (1999) Mater Sci Eng A 270:55
14. Maloney SK, Hono K, Polmear IJ, Ringer SP (1999) Scr Mater 41:1031
15. Engdahl T, Hansen V, Warren PJ, Stiller K (2002) Mater Sci Eng A 327:59
16. Marlaud T, Deschamps A, Bley F, Lefebvre W, Baroux B (2010) Acta Mater 58:248
17. Dumont M, Lefebvre W, Doisneau-Cottignies B, Deschamps A (2005) Acta Mater 53:2881
18. Marlaud T, Deschamps A, Bley F, Lefebvre W, Baroux B (2010) Acta Mater 58:4814
19. Lefebvre W, Da Costa G, De Geuser F, Deschamps A, Danoix F (2007) Surf Interface Anal 39:206
20. Nellist PD, Pennycook SJ (2000) Adv Imaging Electron Phys 113:147
21. Yamazaki T, Kawasaki M, Watanabe K, Hashimoto I, Shiojiri M (2002) Ultramicroscopy 92:181
22. Rose H (2010) Ultramicroscopy 110:488
23. Li YY, Kovarik L, Phillips PJ, Hsu YF, Wang WH, Mills MJ (2012) Philos Mag Lett 92:166
24. Van Aert S, Verbeeck J, Erni R, Bals S, Luysberg M, Van Dyck D, Van Tendeloo D (2009) Ultramicroscopy 109:1236
25. Kresse G, Furthmuller J (1996) Phys Rev B 54:11169
26. Perdew JP, Burke K, Ernzerhof M (1996) Phys Rev Lett 77:3865
27. Pulay P (1980) Chem Phys Lett 73:393
28. Ravi C, Wolverton C (2004) Acta Mater 52:4213
29. Dwyer C, Weyland M, Chang Ly, Muddle BC (2011) Appl Phys Lett 98:2019091